

# Microrobotics Using Composite Materials: The Micromechanical Flying Insect Thorax\*

R. J. Wood      S. Avadhanula      M. Menon      R. S. Fearing  
Department of EECS, University of California, Berkeley, CA 94720  
{rjwood, srinath, manas, ronf}@robotics.eecs.berkeley.edu

## Abstract

*The use of high performance composite materials provides a substantial performance improvement for microrobotics. Such materials have great benefits over common MEMs materials such as better fracture toughness and fatigue properties than semiconductors, and higher stiffness to weight ratios than most metals. Composite structures yield remarkable improvements in microrobotic links and joints, as well as greater performance actuators while allowing complicated microrobotic mechanisms to be easily rapid prototyped. The use of such materials in the construction of the 4DOF, 26 joint Micromechanical Flying Insect has reduced the thorax inertia by a factor of 3 and given a 20% increase in resonant frequency over previous designs while cutting construction time from weeks to days.*

## 1 Introduction

The Micromechanical Flying Insect (MFI) project [2, 7, 11, 12, 15, 16] aims to create an autonomous flying robotic insect the size of a housefly. To do this, biologists have identified mechanisms in real insects which are necessary for flight [5], thus solving the mystery of how insects produce adequate lift for stable flight. The results show that to produce enough lift, while also having a structure which is capable of creating thrust vectors necessary for control of the insect, there are a number of key kinematic and dynamic requirements. The MFI wings must be capable of independently going through a wing stroke of  $120^\circ$ , while being able to rotate  $90^\circ$  at a resonant frequency of  $150Hz$ . To do this the body of the MFI consists of two wings, each driven by separate thorax structures. The thorax structures consist of two actuators, two mechanically amplifying four-bar structures, and a differential. Since the work done on the air is proportional to the velocity of the wing squared, the most important requirements are a high resonant frequency and a large stroke angle.

---

\*This work was funded by ONR MURI N00014-98-1-0671, and DARPA.

One technique for the construction of microrobots uses micromachined silicon for links and hinges as joints [6, 17]. Previous iterations of the MFI thorax have been produced by using stainless steel beams as the structural members and polymer flexures to act as joints. This has the obvious drawbacks of having high inertias, thus lowering the resonant frequency. This also gives rise to a higher mechanical  $Q$  causing a decrease in controllability. The first part of this paper discusses a one degree of freedom (DOF) MFI thorax structure (one-half of a complete thorax), a design for carbon fiber based honey-comb structural beams, a composite wing differential, and a composite beam airframe with the test results for such a device. The second part of this paper discusses a design for a composite based actuator and the results from tests on the actuators.

To keep the weight of the thorax low, the MFI uses unimorph piezoelectric actuators [12]. Such actuators produce large forces and small displacements, thus it is necessary to use a mechanical amplifier to transform these small displacements into large wing strokes. The actuators currently use stainless steel as the elastic layer, thus again causing high inertias and construction problems. By utilizing the high stiffness to weight ratios of composites this inertia can be decreased while allowing for the tailoring of the anisotropy of the layer. This anisotropy makes it possible to create an actuator with kinematic properties that allow simplifications to be made within the kinematics of the four-bar structure.

## 2 Microfabrication of Composite Materials

The first important consideration is the feasibility of using fiber-reinforced materials for the construction of micro devices. The links within the four-bar structure have sizes ranging from  $0.5mm$  to  $6mm$  in length with widths of between  $0.5mm$  to  $1mm$ . Thus for a honeycomb structure, using a cell wall size of an order of magnitude less than the smallest dimension within the thorax gives  $50\mu m$  as the smallest re-

quired beam width. For fiber-reinforced composites with fiber diameters of around  $10\mu m$ , this is approximately the limiting size for these materials.

Using composites for this application assumes the ability to machine the laminates on a single ply basis, down to accuracies of approximately the fiber diameter. Thus traditional methods of cutting and handling these materials is not possible at this scale. Instead, a laser micromachining stage is used to cut the plies, both in a cured and an uncured state. To do this, all plies are designed using a two dimensional CAD package and a laser cuts the plies automatically. For the example application, a material with a high stiffness to weight ratio was desired, thus M60J UHM carbon fiber reinforced epoxy was used. Experimentally, up to two cured plies can be cut simultaneously, or one uncured ply. To eliminate errors during construction of the cut laminae, all angles are controlled within the 2D CAD layout, and the plies are aligned visually under a microscope before cutting. The last concern with laser micromachining these laminae is whether to cut the composite cured or uncured. Using uncured layers to construct the thorax has the great benefit of being able to layup the laminae for the links and a polymer for the joints at one time, and cure this laminate without the need for extra adhesive layers. This simplifies construction, and cuts down on inertia by eliminating the need for any additional epoxy. Laser micromachining an uncured lamina has difficulties since the laser creates localized heating, causing the epoxy matrix to flow around the cutting area, causing the laser to go out of focus. Thus laser cutting uncured lamina is possible, but becomes increasingly more difficult with smaller size parts and is only possible for one layer at a time. Also, since the uncured matrix is still in a viscoelastic state, smaller features can be easily destroyed in handling after cutting. Through careful practice and paying attention to these problems, the MFI thorax has evolved to using a construction based upon using mostly uncured laminae in its layup. Table 1 shows the lamina parameters of each material considered throughout the designs.

**Table 1:** Design parameters for MFI materials.

Parameter	M60J	Steel	Si	Units
$E_1$	350	193	190	$GPa$
$E_2$	7	193	190	$GPa$
$\nu_{12}$	0.33	0.3	0.27	—
$G_{12}$	5	74	75	$GPa$
$t_{UHM}$	25	12.5	—	$\mu m$
$\rho$	1650	7800	2300	$kg \cdot m^{-3}$

### 3 Thorax Construction

The MFI actuators drive a four-bar structure consisting of hollow beams as links and polymer flexures as joints. Between the actuator and four-bar is a slider crack mechanism which converts the approximately linear motion of the tip of the actuator to a rotation at the base of the four-bar. Figure 1 shows a concept of the complete two wing MFI and a mockup structure. The previous MFI links were constructed from stainless steel beams [11]. Since the inertia of the entire thorax is a linear combination of the individual link inertias, using a material with a higher strength to weight ratio will reduce the inertia of the structure. Ideally, this inertia would be reduced by the ratios of the stiffness to weight ratios of the composite to the steel, however, since all designs must include construction issues, the inertia savings will be slightly less than this. For the M60J, the inertia would ideally be reduced by a factor of 10 over stainless steel. The following describes the design of structural members to achieve this savings.

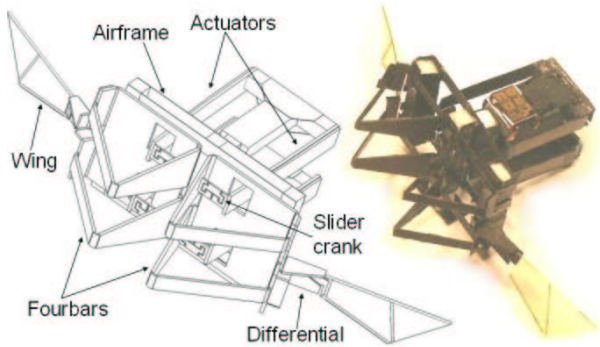


**Figure 1:** 26 joint, 4 actuator, 4DOF, 2 wing MFI.

#### 3.1 Composite Links

For the maximum weight savings, the beams should not be solid structures. Instead, a honeycomb configuration is used, with the M60J as both the face sheet and the core. The analysis done for the beams is aimed at matching the stiffness of the stainless steel beams while minimizing the weight of the beam.

First, the stiffness of a double supported cantilever beam is given by:

$$k = \frac{48EI}{l^3} \quad (1)$$

The current beams have a hollow triangular cross section, with a moment of inertia given by the following:

$$I_t = \frac{\sqrt{3}}{96} \left( B^4 - (B - t_s)^4 \right) \quad (2)$$

The cross sectional moment of inertia of a honeycomb structure is:

$$I_{h1} = \frac{1}{12} (BH^3 - bh^3) \quad (3)$$

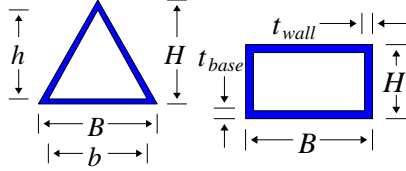


**Figure 2:** (a) Triangular beam cross section and (b) cross section from honeycomb beam.

Figure 2 shows the cross sections defined in (2) and (3). For the parameters of the MFI four-bar with steel beams, the link stiffness is  $3.9 \times 10^4 Nm^{-1}$  and the mass is  $2.34mg$ . The goal is to match this stiffness using the honeycomb structure by optimizing over the geometric parameters shown in Figure 2(b). To simplify this, the parameter  $t_{base}$  is set to  $50\mu m$  since up to two  $25\mu m$  plies can be cut at once. Also, the parameter  $B$  is set to  $1mm$  to allow the four-bar to fit into the current form factor. Thus a two-parameter optimization can be done over  $t_{wall}$  and  $H$ . Note that this is done with the restriction that  $t_{wall}$  cannot be less than the fiber diameter. The results of the optimization are shown in Figure 3.

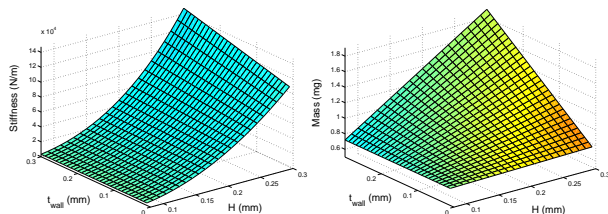


**Figure 3:** (a) Four-bar stiffness and (b) mass as a function of geometric parameters.

From the plot in Figure 3(a), the stiffness was matched to the triangular steel link stiffness and for the given geometric parameters, the mass of the individual link was found to be  $1.16mg$ , which is roughly half the current link mass.

Because of the difficulty in manufacturing and handling the carbon fiber core sections an alternative approach was used in further construction. This entailed the use of the molded polymer core sections shown in the bottom of Figure 4(a). These core sections are easy to produce and handle and bond well to the carbon fiber prepreg. The core shown has  $75\mu m$  wall thicknesses and a  $0.5mm$  depth. Now since the face sheet thickness is much less than the

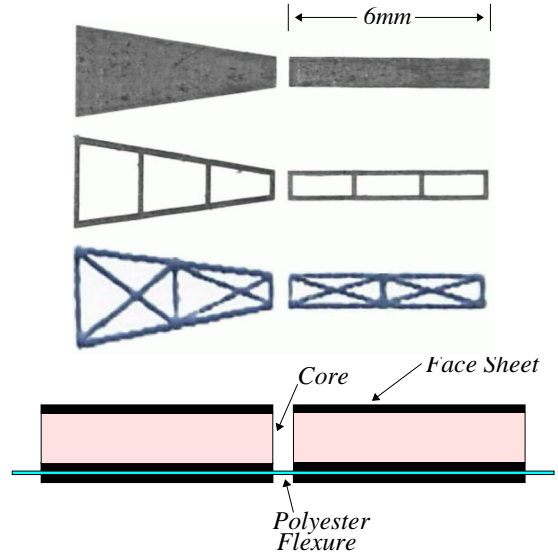


**Figure 4:** (a) Laser micro machined face sheets and honeycomb sections, molded honeycomb core, and (b) layup cross section.

core thickness, the cross sectional moment of inertia is approximated as:

$$I_{h2} = \frac{Bt_f t_c^2}{2} \quad (4)$$

where  $t_f$  is the face sheet thickness and  $t_c$  is the core thickness. Thus the stiffness of this beam is  $3.6 \times 10^5 Nm^{-1}$ , with a mass of  $1.4mg$ .

### 3.2 Joint Fabrication

The four-bar is constructed by sandwiching the polyester flexure layer within the honeycomb structure. Thus there is no need for clamps to prevent peeling, as is the case with the steel beam construction. The final element of the 1DOF thorax is the connection between the actuator and the base link. Since the actuator tip and the base link slider crank attachment point form two intersecting arcs, there need to be additional joints between the two. This is achieved using a traditional slider crank mechanism. The current MFI thorax uses a slider crank which relies upon the buckling strength of the flexures to determine the serial stiffness. Because of the non-linear motions of the actuator and the four-bar base link, this design causes a non-linear decrease in serial stiffness, in effect creating a backlash element. To eliminate this, a no-buckling design was introduced. This concept is shown in Figure 5(a). This slider crank increases the serial stiffness by ensuring that regardless of the position of the elements of the thorax, there will be flexures within the slider crank that are in tension. This concept has been attempted by using the standard steel beam construction, however

it is ineffective since the construction is bulky, requiring too complex a structure to obtain links with the required stiffness. The stiffness of the slider cranks must be higher than the rest of the thorax links since the slider crank will see the highest forces. Also, the complexity of the structure causes alignment errors to arise, leading to kinematic singularities and an increase in the effective parallel stiffness. Thus, if the stiffness of the sections could remain high, while using a planar structure to decrease the complexity, the no-buckling slider crank could be made in a small and efficient form factor.

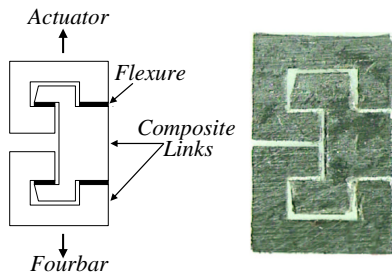


**Figure 5:** (a) Concept drawing and (b) completed no-buckling slider crank.

Figure 5 (b) shows the completed no-buckling slider crank, made with four layers,  $[90/0]_s$  with the polyester flexure layer in the middle. Now the entire 1DOF structure can be completed and is shown in Figure 6.

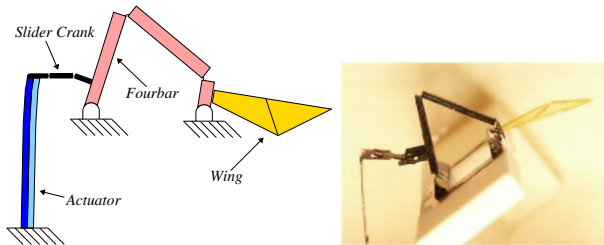


**Figure 6:** (a) Model of and (b) Completed 1DOF composite thorax.

The results of the carbon fiber MFI thorax are compared to results from a steel version with the same dimensions, and using a similar actuator. The two main dynamic parameters which are affected by the lower inertia are the resonant frequency and the mechanical  $Q$ . The  $Q$  is required to be low since it determines the ratio between the inertia force and the aerodynamic force [15]. The resonant frequency is desired to be high since an increase in velocity increases the work done by the wing on the air. Table 2 gives the four-bar parameters for the previous design and the composite structure.

### 3.3 Differential Fabrication

The combined flapping and rotation necessary for flight [5] is from 2-1DOF structures and a differential mechanism which maps the two rotational outputs of the four-bars into a flapping and a rotational wing motion depending upon the amplitude and relative phase of the four-bars [2]. Previously this differential was constructed using similar folding techniques as the four-bars. Thus there could be an improvement not only in the dynamics of the structure, but in the construction by utilizing these composite materials.

The wing differential consists of a spherical five-bar, which allows the two independent four-bar rotations about their individual axes to be converted into the flapping and rotation of the wing. The mechanism consists of five links (two of them the four-bar output links), connected together by flexures. For the mechanism to function properly, the flexure axes have to intersect at a single point. The carbon fiber fabrication process causes such constraints to be achieved very easily and with much better precision than in the previous stainless steel process since none of the flexures are aligned manually. The high stiffness to weight ratio of carbon fiber laminae allows for a differential constructed from two sheets of prepreg with the flexures between. This yields a one-step fabrication process which cuts down fabrication times by an order of magnitude. In the previous stainless steel process, each link had to be manually folded into a triangle. Due to the improved clamping via carbon fiber, the serial stiffness within the differential is increased, along with a 50% decrease in inertia from the lighter composites. Because of this improved clamping the joint motion more closely resembles a pin joint, allowing for much better dynamic control.

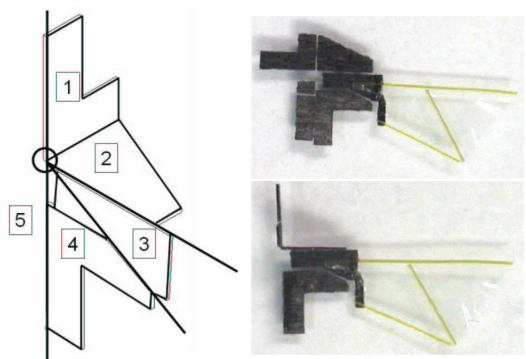


**Figure 7:** Composite wing differential, (a) Spherical 5-bar drawing, (b) planar and (c) folded into 5-bar.

The completed, 2DOF composite MFI thorax is shown in Figure 8. The structure has a flapping resonance at  $160Hz$ , as compared to a previous model constructed from steel beams which resonated at  $133Hz$ .

**Table 2:** Comparison of old and new MFI components.

Parameter	Steel	C.F.	Units
Link Stiff.	0.039	0.360	$N\mu m^{-1}$
Link Mass	2.34	1.40	$mg$
4bar Stiff.(Ser)	140	330	$Nm^{-1}$
4bar Stiff.(Par)	120	90	$Nm^{-1}$
4bar Inertia	20	5	$mg \cdot mm^2$
Diff. Inertia	4	2.5	$mg \cdot mm^2$
$Q$	3.5	2.5	—
$f_{res}(1DOF)$	120	190	$Hz$
$f_{res}(2DOF)$	133	160	$Hz$

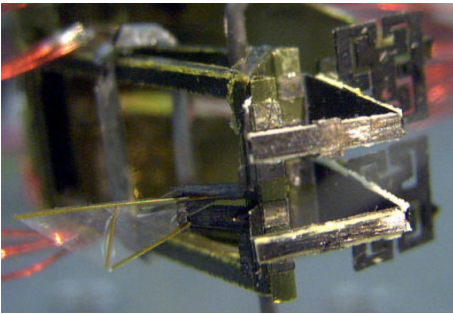


**Figure 8:** One wing 2DOF composite MFI thorax.

### 3.4 Airframe Design

The structure shown in figure 8 is mounted on a steel airframe. Such a structure would be too heavy for flight, thus it is again desired to use the high stiffness-to-weight properties of composite materials in construction of a lightweight airframe. Because of lift power limitations, the mass of this airframe is constrained to  $30mg$ . The airframe needs to behave as a rigid body, and thus should have stiffness at least 10 times that of the actuators. Like the four-bars, the airframe uses molded polyurethane to support and orient the carbon fiber sheets. The  $30mg$  mass restriction limits the application of polyurethane to end caps for the beams of the structure. These end caps are each shaped to fit just inside the end of a specific beam, and are  $1mm$  in depth.

There are two main parts to the airframe. First, the stage holds the four-bars and consists of three parallel box beams that are linked by several planks. Below the stage are two pillars, on which pairs of actuators are mounted. The theoretical stiffness of the stage can be estimated by taking a cross section at critical locations and calculating the stiffness by assuming that both the stage and pillars are single supported cantilevers joined in the center. Such calculations give a stage pillar stiffness of  $2.55 \times 10^5 Nm^{-1}$

and a pillar stiffness of  $4.3 \times 10^6 Nm^{-1}$ . These values are acceptable since a typical actuator has a stiffness on the order of  $150 Nm^{-1}$ . An airframe with this design was constructed that had a mass of  $28mg$ . Figure 9 shows a detail of the airframe for use in the two wing MFI (Figure 1).

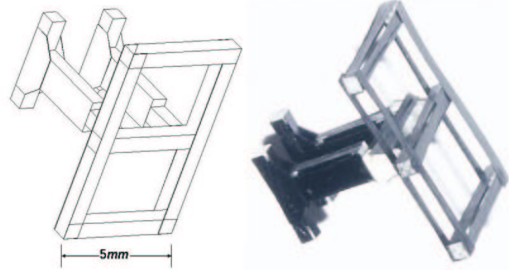


**Figure 9:** (a) Airframe model and (b) completed 28mg airframe.

## 4 Actuator Design

Previous MFI unimorph actuators used stainless steel as an elastic layer [12]. This not only gives a large increase in inertia, but a decrease in functionality because of isotropy and difficulty in machining at this scale. Using a composite elastic layer not only reduces the inertia, but also allows for tailored anisotropy, giving the possibility of interesting kinematic properties. Melz [10] identifies a number of composite structures with embedded piezoelectric plates for shape control and sensing. Kioua in [9] uses a number of discrete piezoelectric plates to control the shape of such a unimorph actuator. However, since the kinematics of the four-bar are simple and constant, control of such a structure is difficult, and since such a structure will be less efficient than a traditional piezoelectric actuator, it is desired to have passive shape control by utilizing non-standard ply layups. The first objective is to create an actuator with greater performance and ease of construction than the current MFI actuators. The second objective is to utilize the anisotropy inherent in composite materials to create an actuator whose kinematics eliminate the need for certain joints within the slider crank and four-bar structure. This will be done by maximizing bending-twisting coupling in a fashion similar to the analysis of Zhu [18] with extension-twisting coupling. Figure 10 shows a detail of the actuator layers.

First, consider that the actuator consists of two components, a piezoceramic layer and an elastic layer. Applying an electric field to the piezo layer creates a strain in a free plate. Since the piezo motion is restricted by the elastic layer, a stress develops. This stress within the actuator varies through the cross

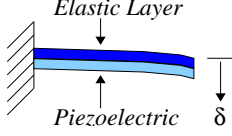


**Figure 10:** Detail of unimorph actuator layers.

section of the actuator, thus there is an effective moment in the beam, causing a deflection. The strain in the piezo layer is given by the following:

$$\epsilon_1^p = \frac{1}{E_p} \sigma_1^p - d_{31} \frac{V_{app}}{t} \quad (5)$$

where  $d_{31}$  is the piezoelectric constant and  $V_{app}$  is the applied voltage. More generally, this strain is given in the following form:

$$\begin{bmatrix} \epsilon_1 \\ \epsilon_2 \\ \gamma_{12} \end{bmatrix}_p = \begin{bmatrix} Q_{11} & Q_{12} & 0 \\ Q_{12} & Q_{22} & 0 \\ 0 & 0 & Q_{66} \end{bmatrix}_p^{-1} \begin{bmatrix} \sigma_1 \\ \sigma_2 \\ \tau_{12} \end{bmatrix}_p - \begin{bmatrix} d_{31} \\ d_{32} \\ 0 \end{bmatrix} \frac{V_{app}}{t} \quad (6)$$

Using the assumption that the piezoelectric layer is transversely isotropic ( $d_{31} = d_{32}$ ),  $d_{36}$  is taken to be 0 thus there is no shearing forces or twisting moments applied by the piezoelectric [9]. Solving (6) for the stresses in the piezo layer gives the following:

$$\begin{bmatrix} \sigma_1 \\ \sigma_2 \\ \tau_{12} \end{bmatrix}_p = \begin{bmatrix} Q_{11} & Q_{12} & 0 \\ Q_{12} & Q_{22} & 0 \\ 0 & 0 & Q_{66} \end{bmatrix}_p \cdot \left( \begin{bmatrix} \epsilon_1 \\ \epsilon_2 \\ \gamma_{12} \end{bmatrix}_p - \begin{bmatrix} d_{31} \\ d_{32} \\ 0 \end{bmatrix} \frac{V_{app}}{t} \right) \quad (7)$$

In equations (6) and (7), the  $[Q_{ij}]_p$  terms are the material constants of the piezo as given in Table 3. Similarly, the stresses in the elastic layer are given as follows:

$$\begin{bmatrix} \sigma_1 \\ \sigma_2 \\ \tau_{12} \end{bmatrix}_e = \begin{bmatrix} Q_{11} & Q_{12} & 0 \\ Q_{12} & Q_{22} & 0 \\ 0 & 0 & Q_{66} \end{bmatrix}_e \begin{bmatrix} \epsilon_1 \\ \epsilon_2 \\ \gamma_{12} \end{bmatrix}_e \quad (8)$$

Now the forces and moments (per unit width) are given as a function of the ply stresses:

$$\begin{aligned} [N_{ij}] &= \int_0^h [\sigma_{ij}] dz \\ [M_{ij}] &= \int_0^h [\sigma_{ij}] z dz \end{aligned} \quad (9)$$

In (9), the term  $h$  is the total actuator thickness, thus to solve for  $N_{ij}$  and  $M_{ij}$  the integrals need to be split into a summation over all layers of the actuator.

$$\begin{aligned} [N_{ij}] &= \sum_k \int_{t_{k-1}}^{t_k} [\sigma_{ij}]_k dz \\ [M_{ij}] &= \sum_k \int_{t_{k-1}}^{t_k} [\sigma_{ij}]_k z dz \end{aligned} \quad (10)$$

Next, the actuator properties are determined as a function of the ply layout using laminate plate theory. For simplicity, this is done so that the actuator provides roughly the same displacement and has the same stiffness as the current MFI actuators. First, the relationship between the midplane strains and curvatures and the forces and moments are given by:

$$\begin{bmatrix} N \\ M \end{bmatrix} = \begin{bmatrix} A_{ij} & B_{ij} \\ B_{ij} & D_{ij} \end{bmatrix} \begin{bmatrix} \epsilon^0 \\ \kappa \end{bmatrix} - \begin{bmatrix} N^p \\ M^p \end{bmatrix} \quad (11)$$

In (11)  $N$  and  $M$  are the external forces and moments acting on the actuator, and  $N^p$  and  $M^p$  are the piezoelectric forces and moments generated within the actuator. Also, the  $A$ ,  $B$ , and  $D$  terms are given as follows:

$$\begin{aligned} A_{ij} &= \sum_k [Q_{ij}]_k (z_k - z_{k-1}) \\ B_{ij} &= \frac{1}{2} \sum_k [Q_{ij}]_k (z_k^2 - z_{k-1}^2) \\ D_{ij} &= \frac{1}{3} \sum_k [Q_{ij}]_k (z_k^3 - z_{k-1}^3) \end{aligned} \quad (12)$$

Next assume that there are no external forces and moments, that is assume that all extension and curvature is a result of the piezoelectric effect. Now for this application, there are two terms of importance within (11), the curvature in the displacement direction,  $\kappa_x$  and the twist curvature,  $\kappa_{xy}$ . These two quantities are related to the linear displacement of the tip of the actuator and the output twist angle as follows:

$$\begin{aligned} \delta &= \frac{1}{2} \kappa_x l^2 \\ \gamma &= \arctan \left( \kappa_{xy} \left( \frac{l^2 + w^2}{w} \right) \right) \end{aligned} \quad (13)$$

where  $\delta$  is the linear displacement of the tip of the actuator in meters, and  $\gamma$  is the output twist angle in radians.

The MFI actuators use both amorphous (PZT) and single crystal (PZN-PT) piezoceramics. Two designs here will be discussed, first an actuator using the PZN-PT with only bending, and second a PZT based actuator with simultaneous bending and twisting. Both design use UHM M60J as the elastic layer. The

only design parameter for the first actuator is the stiffness since this must match a desired value for the proper dynamics. Because of the simplicity of this actuator, the details of the design are omitted. However for a  $100\mu\text{m}$  thick PZN-PT layer, and a desired stiffness of  $150\text{Nm}^{-1}$ ,  $25\mu\text{m}$  of UHM are needed for an actuator with dimensions of  $7\text{mm} \times 1.8\text{mm}$  with a  $1.5\text{mm}$  extension. Such an actuator will give approximately  $740\mu\text{m}$  displacement,  $112\text{mN}$  blocked force and an energy density of  $3.5\text{Jkg}^{-1}$  at  $250\text{V}$ .

By exploiting the anisotropy of composites, it is possible to design and build actuators with a passive twist at the free end of the beam. This could be used to eliminate some joints within the thorax, thus simplifying the structure. Because of the desired kinematics of the wing, it is desired to have  $\gamma$  be as large as possible while keeping  $\delta$  roughly the same as the current actuators. Because of the large number of variables involved, an analytic approach to solving for the lamina layup angles was avoided. Instead, a numerical approach was used which generated  $\delta$  and  $\gamma$  as a function of the layup for a standard given input voltage. This was done using a script which searched a confined parameter space and determined the optimum  $\delta$  and  $\gamma$  for each iteration. The results of this search gave a layup of  $[\text{piezo}/\theta/0/0/\theta]$ , where  $\theta$  are the ply angles. For this layup,  $\delta$  and  $\gamma$  are given in Figure 11 as a function of  $\theta$ .

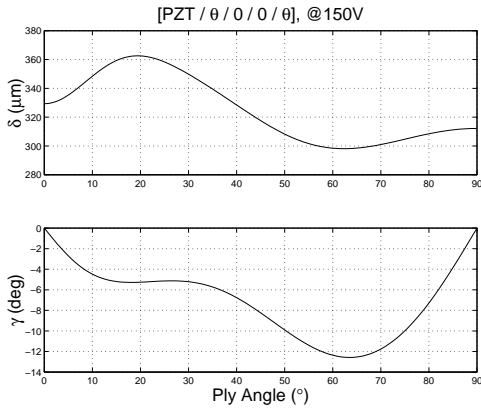


**Figure 11:** Displacement and twist angle as a function of layup.

From the results in Figure 11, it is shown that the maximum output twist angle occurs when  $\theta = 63^\circ$ , which corresponds to  $\gamma = 12^\circ$ , and  $d = 300\mu\text{m}$ , which is approximately the same displacement as the current actuators. For these parameters, a four-bar transmission ratio of 10 will give the desired output angle of  $120^\circ$ . Also, Figure 11 shows that the twist and displacement are robust to small changes in the ply angles. Figure 12 shows a simulated end-on view of the actuator through one cycle.

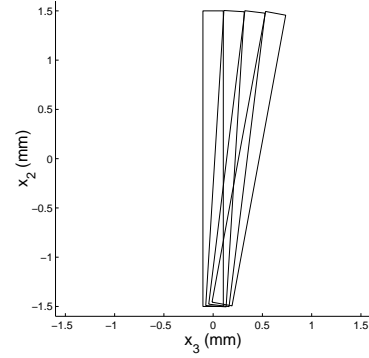


**Figure 12:** End on view of the actuator through one complete cycle.

To test the analysis and simulation results, actuators were constructed using the principles described in section 4 and the layup calculated above. These actuators gave an average displacement of approximately  $400\mu\text{m}$ , and an average twist angle of  $6^\circ$ . This is still acceptable however since all analysis was done for static conditions, however with a mechanical  $Q$  of 2 or greater (which is always the case with recent structures), the desired kinematic properties can be met. Table 3 shows the material and electrical properties of the two types of piezoceramics used in the MFI actuators.

**Table 3:** Piezoelectric properties.

Parameter	PZT	PZN-PT	Units
$E_1$	61	15	$\text{GPa}$
$\nu_{12}$	0.28	0.26	—
$G_{12}$	25	6	$\text{GPa}$
$t_p$	127	100	$\mu\text{m}$
$d_{31}$	-320	-950	$\text{pC}\text{N}^{-1}$

## 5 Summary and Future Work

The use of fiber reinforced laminates provides significant inertia reduction in both macro and micro robotics applications. Until recently, the use of such materials has been restricted to larger scale applications because of manufacturing difficulties inherent in the laminae. This paper suggests a novel method of machining and assembling the individual layers for use in microrobotics. The resulting structures consist of lighter, stiffer links with joints that behave more accurately as pin joints. This result, along with high power density composite actuators, forms a class of microstructures which enable high performance microrobots.

The benefits of these materials for the MFI is two-fold. First the serial stiffness is greatly increased since the lamina matrix bonds well to the polyester

flexures used in the MFI. This also eases construction by eliminating the need for any additional epoxy. The second benefit comes from the greater stiffness-to-weight ratios of these structures over other materials used in microrobotics. For example, for 1mm wide, 6mm long beams, a beam constructed from folded triangle of 12.5 $\mu$ m thick steel will have a stiffness-to-weight ratio of  $4.5 \times 10^{10} Nm^{-1}kg^{-1}$  compared to a hinged silicon folded triangle beam similar to the one described by Yeh [17] at  $1.5 \times 10^{11} Nm^{-1}kg^{-1}$ , and  $2.6 \times 10^{11} Nm^{-1}kg^{-1}$  for the composite beam.

For use within the MFI four-bar structure, the UHM M60J gives structures which for a given stiffness, reduces the mass by a factor of three compared to folded 12.5 $\mu$ m steel. Similarly, when used in the actuator, the inertia is reduced while allowing for bending-twisting coupling to eliminate some of the complexity of the thorax. Future work will include the composite actuators in the thorax, connected directly to the four-bar, eliminating the slider crank.

Other future work will involve an improvement of the layup analysis described in section 4. This analysis was done by using a search over a restricted parameter space, that is the ply angles were limited to either 0 or  $\pm\theta$ . To improve the results of this search, the parameterization should be global, that is search over all possible combinations of layup angles. Since such a search would require large amounts of computation time, it will be better to use a learning algorithm to determine the actuator layup.

### Acknowledgments

The authors would like to thank Prof. Hari Dharan and the Berkeley Composites Laboratory for the use of materials and equipment.

### References

- [1] O. J. Aldraihem and R. C. Wetherhold. Mechanics and control of coupled bending and twisting vibration of laminated beams. *J of Smart Materials and Structures*, vol. 6, pages 123-133, 1997.
- [2] S. Avadhanula, R. J. Wood, D. Campolo, and R. S. Fearing. Dynamically tuned design of the MFI thorax. *IEEE Intl Conf on Robotics and Automation*, Washinton, DC, May 11-15, 2002.
- [3] J. C. Bruch Jr, J. M. Sloss, S. Adali, and I. S. Sadek. Optimal piezo-actuator locations/lengths and applied voltage for shape control of beams. *J of Smart Materials and Structures*, vol. 9, pages 205-211, 2000.
- [4] A. Cox, M. Goldfarb, and E. Garcia. Actuator development for a flapping microrobotic microaerial vehicle. *Microrobotics and Micromanipulation, Proceedings of SPIE*, vol. 3519, pp. 102-108, November 1998.
- [5] M.H. Dickinson, F-O. Lehmann, and S. P. Sane. Wing rotation and the basis for insect flight. *Science*, 284:1954-960, June 1999.
- [6] T. Ebefors, J. Mattson, E. Kalvesten, and G. Steme. A walking silicon micro-robot. *10<sup>th</sup> Intl Conf on Solid-State Sensors and Actuators (TRANSDUCERS '99)*, pp. 1202-1205, Sendai, Japan, June 7-10, 1999.
- [7] R.S. Fearing, K.H. Chiang, M.H. Dickinson, D.L. Pick, M. Sitti, and J. Yan. Wing transmission for a micromechanical flying insect. *IEEE Intl Conf on Robotics and Automation*, pages 1509-1516, San Francisco, CA, April 2000.
- [8] J.H. Han, K.D. Cho, S.H. Youn, and I. Lee. Vibration characteristics of composite structures with a bonded piezo-ceramic actuator. *J of Smart Materials and Structures*, vol. 8, pages 136-143, 1999.
- [9] H. Kioua, S. Mirza. Piezoelectric induced bending and twisting of laminated composite shallow shells. *J of Smart Materials and Structures*, vol. 9, pages 476-484, 2000.
- [10] T. Melz, P. Wierach, D. Sachau, V. Krajenski, G. Mook, and H. Hanselka. Carbon fiber composite materials with structural conformable integrated piezoelectric for adaptive structures. *9<sup>th</sup> Intl Conf on Adaptive Structures and Technologies*, Technomic Publishing. 1999, pp.137-46. Lancaster, PA, USA.
- [11] E. Shimada, J.A. Thompson, J. Yan, R.J. Wood, and R.S. Fearing. Prototyping millirobots using dexterous microassembly and folding. *Symp on Microrobotics ASME Intl Mech Eng Cong and Expo*, Orlando, FL, Nov 5-10, 2000.
- [12] M. Sitti, D. Campolo, J. Yan, R.S. Fearing, T. Su, D. Taylor. Development of PZT and PZN-PT based unimorph actuators for micromechanical flapping structures. *IEEE Intl Conf on Robotics and Automation*, Seoul, Korea, May 2001.
- [13] J. Smits and W. Choi. The constituent equations of piezoelectric heterogeneous bimorphs. *IEEE Tran. On Ultrasonics, Ferroelectrics, and Freq. Control*, vol. 38, pages 256-270, May 1991.
- [14] M. Weinberg. Working equations for piezoelectric actuators and sensors. *J of MEMS*, vol. 8, pages 529-533, Dec. 1999.
- [15] R.J. Wood and R.S. Fearing. Flight force measurements for a micromechanical flying insect. *IEEE Conf on Intelligent Robots and Systems*, Maui, HI, Oct. 29-Nov. 3, 2001.
- [16] J. Yan, R.J. Wood, S. Avadhanula, M. Sitti, and R.S. Fearing. Towards flapping wing control for a micromechanical flying insect. *IEEE Intl Conf on Robotics and Automation*, Seoul, Korea, May 2001.
- [17] R. Yeh, E.J.J. Kruglick, and K.S.J. Pister. Surface-micromachined components for articulated micro-robots. *J of MEMS*, vol. 5, no. 1, pp. 10-17, March 1996.
- [18] M-L. Zhu, S-W.R. Lee, H-L. Li, T-Y. Zhang, and P. Tong. Modeling of torsional vibration induced by extension-twisting coupling of anisotropic composite laminates with piezoelectric actuators. *J of Smart Mater. and Struct.*, vol. 11, no. 1, pp. 55-62, Feb. 2002.